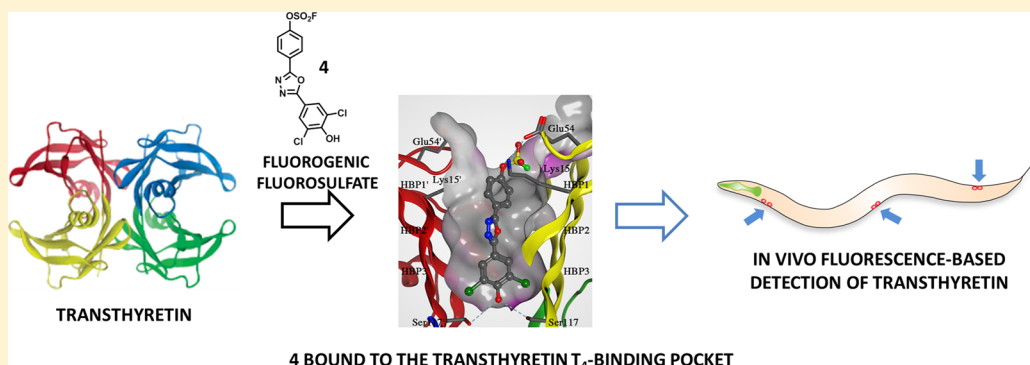


# A Fluorogenic Aryl Fluorosulfate for Intraorganellar Transthyretin Imaging in Living Cells and in *Caenorhabditis elegans*

Aleksandra Baranczak,<sup>†,‡</sup> Yu Liu,<sup>†,‡</sup> Stephen Connelly,<sup>‡,¶</sup> Wen-Ge Han Du,<sup>§</sup> Erin R. Greiner,<sup>†,‡</sup> Joseph C. Genereux,<sup>†,‡</sup> R. Luke Wiseman,<sup>‡,||</sup> Yvonne S. Eisele,<sup>†,‡</sup> Nadine C. Bradbury,<sup>§</sup> Jiajia Dong,<sup>†</sup> Louis Noddleman,<sup>§</sup> K. Barry Sharpless,<sup>†,‡</sup> Ian A. Wilson,<sup>§,#</sup> Sandra E. Encalada,<sup>\*,‡,†,||</sup> and Jeffery W. Kelly<sup>\*,†,‡,‡</sup>

<sup>†</sup>Department of Chemistry, <sup>‡</sup>Department of Molecular and Experimental Medicine, <sup>§</sup>Department of Integrative Structural and Computational Biology, <sup>||</sup>Department of Chemical Physiology, <sup>†</sup>Department of Molecular and Cellular Neuroscience, <sup>#</sup>The Skaggs Institute for Chemical Biology, <sup>||</sup>Dorris Neuroscience Center, The Scripps Research Institute, 10550 North Torrey Pines Road, La Jolla, United States

Supporting Information



**ABSTRACT:** Fluorogenic probes, due to their often greater spatial and temporal sensitivity in comparison to permanently fluorescent small molecules, represent powerful tools to study protein localization and function in the context of living systems. Herein, we report fluorogenic probe 4, a 1,3,4-oxadiazole designed to bind selectively to transthyretin (TTR). Probe 4 comprises a fluorosulfate group not previously used in an environment-sensitive fluorophore. The fluorosulfate functional group does not react covalently with TTR on the time scale required for cellular imaging, but does red shift the emission maximum of probe 4 in comparison to its nonfluorosulfated analogue. We demonstrate that probe 4 is dark in aqueous buffers, whereas the TTR·4 complex exhibits a fluorescence emission maximum at 481 nm. The addition of probe 4 to living HEK293T cells allows efficient binding to and imaging of exogenous TTR within intracellular organelles, including the mitochondria and the endoplasmic reticulum. Furthermore, live *Caenorhabditis elegans* expressing human TTR transgenically and treated with probe 4 display TTR·4 fluorescence in macrophage-like coelomocytes. An analogue of fluorosulfate probe 4 does react selectively with TTR without labeling the remainder of the cellular proteome. Studies on this analogue suggest that certain aryl fluorosulfates, due to their cell and organelle permeability and activatable reactivity, could be considered for the development of protein-selective covalent probes.

## INTRODUCTION

While temporal and spatial localization of a protein-of-interest (POI) has historically been accomplished by fusing the POI to a fluorescent protein or small-molecule-regulated fluorescent protein tag,<sup>1–9</sup> there is growing interest in the development of fluorogenic small molecule probes that directly target proteins-of-interest (PsOI). Fluorogenic probes are defined as fluorophores exhibiting a fluorescent signal only upon binding to or reacting with the POI in the context of a complex biological environment.<sup>10–17</sup> While notable success with fluorogenic probes has been realized, several challenges remain. For example, the majority of fluorogenic probes published to date target enzymes.<sup>4,7,14,18–24</sup> It would be ideal

if fluorogenic probes could be routinely developed for nonenzyme proteins and other macromolecules.<sup>8,13,15,16,25–30</sup> Moreover, a better understanding of the physicochemical underpinnings of fluorogenicity would enable more efficient design.<sup>18,31,32</sup> Numerous applications are expected to result from the development of fluorogenic small molecule probes for important PsOI. For example, probes exhibiting good cell permeability, POI binding selectivity, fast labeling kinetics (assuming covalent probes are sought), and desirable excitation and emission wavelengths can be applied in the design of pulse-

Received: March 23, 2015

Published: June 8, 2015

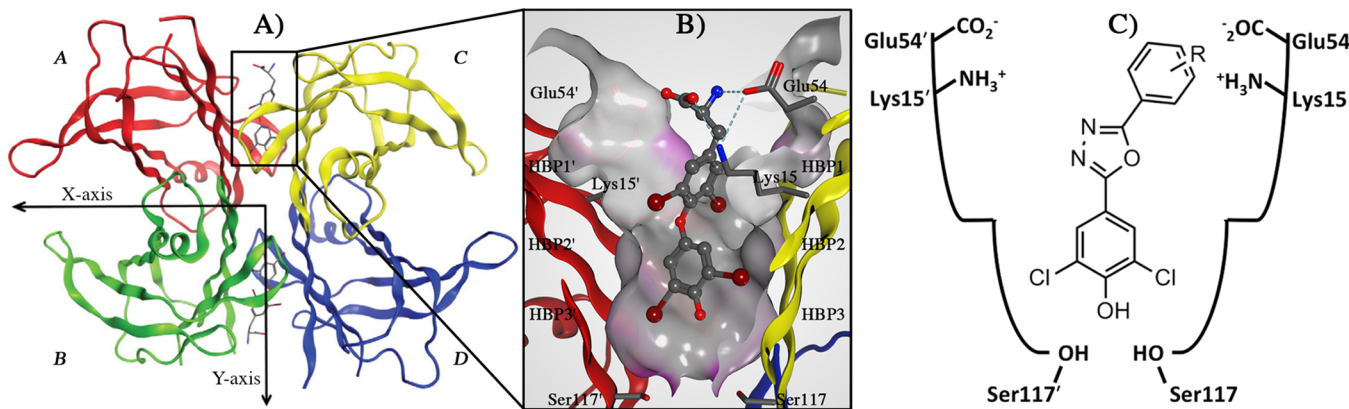


**Figure 1.** Structure of homotetrameric TTR<sup>WT</sup> and its T<sub>4</sub>-binding pockets. (A) Crystal structure of TTR<sup>WT</sup> in complex with two thyroxine (T<sub>4</sub>) molecules (PDB 2ROX).<sup>43</sup> (B) Close-up view of one of the two identical T<sub>4</sub>-binding sites showing a ribbon diagram depicted tetramer (colored by chain) with a “Connolly” molecular surface applied to residues within 8 Å of T<sub>4</sub> (hydrophobic = gray, polar = purple). The innermost halogen binding pockets (HBPs) 3 and 3' are composed of the methyl and methylene groups of Ser117/117', Thr119/119', and Leu110/110'. HBPs 2 and 2' are formed by the side chains of Leu110/110', Ala109/109', Lys15/15', and Leu17/17'. The outermost HBPs 1 and 1' are lined by the methyl and methylene groups of Lys15/15', Ala108/108', and Thr106/106'. These figures were generated using the program MOE (2011.10). (C) Schematic representation of the T<sub>4</sub>-binding pocket with the TTR amino acids that are being targeted in the design and optimization of fluorogenic probes. R = SO<sub>2</sub>F or OSO<sub>2</sub>F.

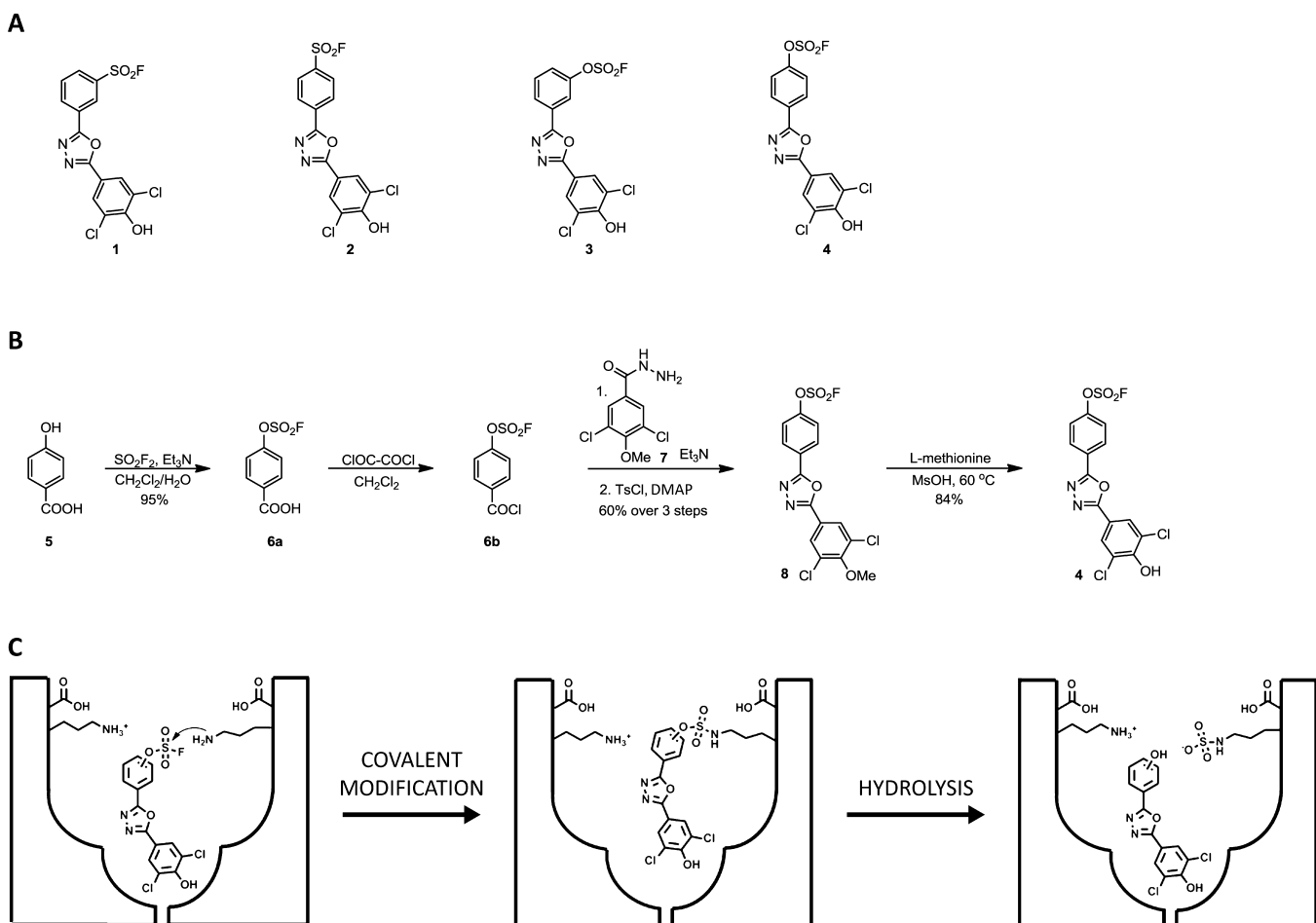


**Figure 2.** (A) Chemical structures of probes 1–4. (B) Synthesis of fluorosulfate 4. (C) An illustration of the fate of some fluorosulfates such as probe 3 in the T<sub>4</sub>-binding pocket. TTR and probe 3 initially form a noncovalent complex. Then reaction of the fluorosulfate group with the Lys15 residue leads to the formation of a TTR-ligand conjugate, which subsequently undergoes hydrolysis to produce sulfamated TTR and the noncovalently bound phenol hydrolysis product, a reaction that may be catalyzed by TTR.

chase experiments within cells to follow POI trafficking and degradation kinetics.

Several different mechanisms contribute to fluorogenicity in small molecules.<sup>18,32</sup> One origin requires an environment-

sensitive (solvatochromic) chromophore, whose fluorescent properties (excitation and emission wavelengths, quantum yields, etc.) depend both on the structure of the chromophore and on the microenvironment of the protein binding site. Environment-sensitive fluorophores are generally dark in aqueous solution, but fluoresce when the chromophore is placed in a hydrophobic membrane environment or in a hydrophobic protein binding site.<sup>10,33–35</sup>

We are interested in developing solvatochromic fluorogenic probes to study the protein transthyretin. Transthyretin (TTR) is a nonenzyme protein synthesized by the liver for secretion into the blood and produced by the choroid plexus for secretion into the cerebrospinal fluid.<sup>36</sup> TTR serves as a transporter of holo-retinol-binding protein and/or thyroxine depending on its localization.<sup>36,37</sup> TTR is composed of 127-amino-acid,  $\beta$ -sheet-rich subunits that associate into a tetramer (Figure 1). Tetramer dissociation is rate limiting for TTR aggregation, which drives the pathology of several degenerative diseases.<sup>38</sup> The dimer–dimer interface bisected by the C<sub>2</sub> or Y axis creates the two funnel-shaped thyroxine (T<sub>4</sub>)-binding sites that are >99% unoccupied, except in tissues bathed by the cerebrospinal fluid<sup>39</sup> (Figure 1A and B).

We have used fluorogenic TTR probes to understand how the cellular proteostasis network affects TTR folding efficiency,<sup>17</sup> and to quantify the kinetic stabilization (measured by the rate of TTR dissociation) afforded by oral tafamidis or diflunisal treatment (drugs that prevent amyloidogenesis).<sup>40–44</sup> Encouraged by the development of TTR-selective fluorogenic probes for the aforementioned uses, as well as for additional applications,<sup>15,16,25,35</sup> we explored the design of additional environment-sensitive, cell-permeable fluorogenic TTR probes wherein the little studied aryl fluorosulfate group (ArOSO<sub>2</sub>F) is incorporated.<sup>45</sup>

Previously, we reported the fluorogenic 1,3,4-oxadiazole-based sulfonyl fluoride **1** (Figure 2A), that upon binding and subsequent reaction with the pK<sub>a</sub>-perturbed Lys-15  $\epsilon$ -amino group within the two thyroxine binding sites of the TTR tetramer creates a fluorescent conjugate.<sup>25</sup> The goal of this study was to evaluate the applicability of 1,3,4-oxadiazole-based aryl fluorosulfates as fluorogenic TTR probes. 1,3,4-oxadiazole-based aryl fluorosulfates were employed to assess the localization of natively folded tetrameric TTR within transgenic *Caenorhabditis elegans*, and to assess their potential to react with TTR,<sup>15,16,25</sup> as well as to examine their general proteome reactivity in cells. Herein, we report on a *para*-sulfonyl fluoride **2** not studied previously, as well as structurally analogous aryl fluorosulfate candidate probes **3** and **4** (Figure 2A). Candidate probe **4** is an environment-sensitive fluorophore that selectively binds to TTR and renders the TTR-**4** complex fluorescent in subcellular compartments of living cells and within coelomocytes of living worms. Unlike probes **1–3**, probe **4** does not react covalently with TTR significantly on the time scale of the imaging experiments.

## EXPERIMENTAL SECTION

**Crystallization and Structure Determination of TTR WT Complexes.** TTR<sup>WT</sup> was concentrated to 6.94 mg/mL in 10 mM sodium phosphate buffer (pH 7.6) with 100 mM KCl and cocrystallized at room temperature with a 5 molar excess of each candidate ligand (2.5 molecules per T<sub>4</sub>-binding site) using the vapor-diffusion sitting drop method. All crystals were grown from 1.395 M sodium citrate, 3.5% v/v glycerol at pH 5.5 as the mother liquor and appeared after 1 week. The crystals were cryo-protected with mother liquor containing 10% v/v glycerol.

Data were collected at beamline 11–1 at the Stanford Synchrotron Radiation Lightsource (SSRL) at a wavelength of 0.9795 Å. All diffraction data were indexed, integrated, and scaled using HKL2000 in orthorhombic space group P2<sub>1</sub>2<sub>1</sub>2 with two promoters per asymmetric unit (half a tetramer).<sup>46</sup> Model building and refinement was carried out using Coot and Refmac5.<sup>47,48</sup> Ligand coordinate and restraint files were generated using JLigand and ligands were assigned an occupancy of 0.5 to account for the ligand residing on the C<sub>2</sub> axis.<sup>49</sup> Hydrogens were added during refinement, and anisotropic B-values were calculated. Final models were validated using the JCSG quality control server v2.8 (<http://smb.slac.stanford.edu/jcsg/QC/>) incorporating MolProbity, ADIT (<http://rcsb-deposit.rutgers.edu/validate>) WHAT-IF, and Resolve.<sup>50–52</sup> Data collection and refinement statistics are summarized in Table S2.

**Confocal Fluorescence Microscopy Detection of TTR in Cultured Live Cells.** For Figure 5, HEK293T cells were plated on chambered coverglasses (Thermo-Fischer) ~20 h after transfection. After 24 h, fresh DMEM (FBS-free) containing MitoTracker Orange CMTMRos (Life Technologies, 500 nM) and NucRed Live 647 Ready Probes Reagent (Life Technologies, solution prepared according to manufacturer's recommendations) and probe **4** (20  $\mu$ M) was added and the cells were incubated at 37 °C under 5% CO<sub>2</sub>. After 20 min, fresh DMEM (FBS-free) was added. After 30 min incubation at 37 °C, DMEM was replaced with DPBS and the cells were imaged using a Zeiss LSM 710 laser scanning confocal microscope (LSCM) attached to a Zeiss Observer Z1 microscope equipped with the infinity corrected optics: 63 $\times$  oil Plan Apo, 1.4na DIC. The following lasers were used for imaging: 405 nm excitation for detection of probe **4**, 561 nm excitation for detection of MitoTracker Orange, and 633 nm excitation for detection of NucRed. Appropriate holistic prism based emission was used to detect the signal of each of the dyes, respectively. For Figures 6 and 7, HEK293T cells were plated in chambered coverglasses (Thermo-Fischer) ~20 h after transfection. After 24 h, fresh DMEM (FBS-free) containing MitoTracker Orange (500 nM) or ER-Tracker Red (1  $\mu$ M) and NucRed (solution prepared according to manufacturer's recommendations) was added and the cells were incubated at 37 °C under 5% CO<sub>2</sub>. After 20 min, DMEM was replaced with DPBS containing probe **4** (5  $\mu$ M). After ~30 s, a fresh solution of DMEM (FBS-free) was added. After 10–15 min, DMEM was replaced with DPBS and the cells were imaged as above.

**C. elegans Methods and Strains.** N2 Bristol was used as the wild-type strain; standard nematode culture methods and genetics were followed as described previously.<sup>53</sup> Nematodes were grown on NGM plates seeded with the *Escherichia coli* strain OP50 at 20 °C. The following transgenic strains were used: CL2008 him-5(e1490) V; dvIs3[unc-54p::hTTR(WT) + rol-6] was provided by C. Link (University of Colorado). The strain CX11480 kyEx3017[des-2p::myr::gfp + unc-122p::DsRed] was provided by C. Bargmann (Rockefeller University). Integration of kyEx3017 was done by gamma irradiation following standard methods.<sup>54</sup> Integrated strains were backcrossed at least four times into an N2 wild-type background. The strain LG398 gels101[rol-6(su1006)] was ordered from the *Caenorhabditis* Genetics Center (CGC). The following strains were made for live-imaging with probe **4**: SEE055 gels101[rol-6(su1006)]; kyEx3017[des-2p::myr::gfp + unc-122p::DsRed] and SEE084 him-5(e1490) V; dvIs3[unc-54p::hTTR(WT) + rol-6]; scrIs010[des-2p::myr::gfp + unc-122p::DsRed].

**In Vivo C. elegans Imaging.** Ten L4 larvae of each of the two strains SEE055 gels101[rol-6(su1006)]; kyEx3017[des-2p::myr::gfp + unc-122p::DsRed] and SEE084 him-5(e1490) V; dvIs3[unc-54p::hTTR(WT) + rol-6]; scrIs010[des-2p::myr::gfp + unc-122p::DsRed] were transferred into a 96-well plate containing 150  $\mu$ L of liquid culture media (S-complete media with 50  $\mu$ g/mL carbenicillin, 0.1  $\mu$ g/mL amphotericin B, 5 mg/mL OP50, 120 nM fluorodeoxyuridine).<sup>55</sup> Worms were mixed on a nutator and incubated overnight at 20 °C. On day 1 of adulthood, probe **4** (0.5  $\mu$ L of a 3 mM solution in DMSO) was added to the worm solution (final concentration 10  $\mu$ M). Worms were mixed well on a nutator and incubated overnight at 20 °C. On day 2 of adulthood, worms were collected and washed three times in 1

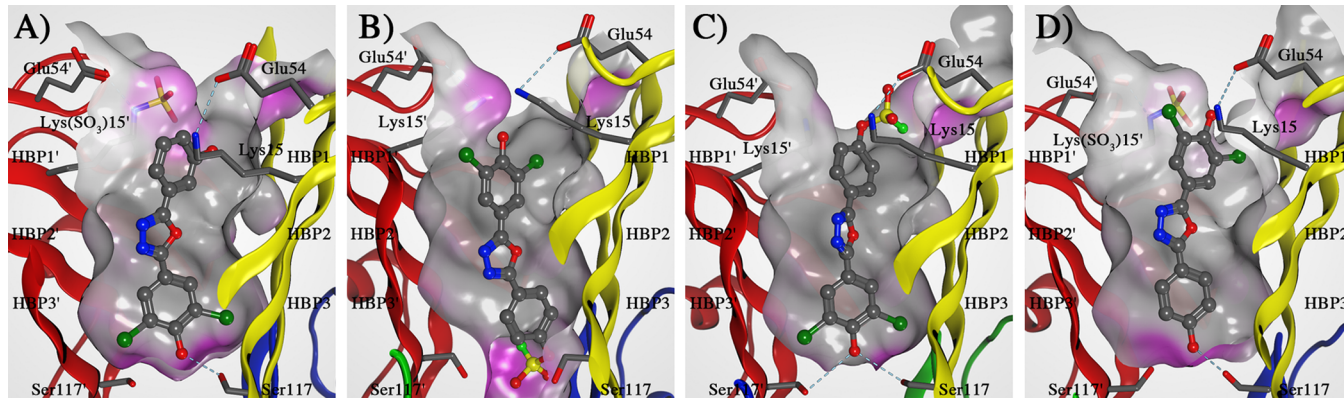


**Figure 3.** Crystal structures of homotetrameric TTR<sup>WT</sup> after binding and/or reaction with probe 3 or probe 4. (A) The product after probe 3 reacted with TTR<sup>WT</sup>. (B) Probe 4 bound in the “forward” orientation. (C) Probe 4 bound in the “reverse” orientation. (D) The product of the very slow reaction between probe 4 and TTR<sup>WT</sup>. Each panel represents a close-up view of one of the two identical T<sub>4</sub>-binding sites as a ribbon diagram depicted tetramer colored by chain. A “Connolly” molecular surface was applied to residues within 8 Å of ligand in the T<sub>4</sub>-binding pocket; hydrophobic (gray), polar (purple). The innermost HBPs 3 and 3' are composed of the methyl and methylene groups of Ser117/117', Thr119/119', and Leu110/110'. HBPs 2 and 2' are formed by the side chains of Leu110/110', Ala109/109', Lys15/15', and Leu17/17'. The outermost HBPs 1 and 1' are lined by the methyl and methylene groups of Lys15/15', Ala108/108', and Thr106/106'. Hydrogen bonds are shown in light blue dashed lines. This figure was generated using the program MOE (2011.10), Chemical Computing Group, Montreal, Canada.

mL of M9 buffer and transferred to a fresh 6 cm NGM plate prior to image analysis.

For light and fluorescence microscopy, animals were mounted in 2% sodium azide buffer (prepared in 1× PBS) on 3% agarose pads and covered with a coverslip. Imaging of coelomocytes was done on live animals with simultaneous differential interference contrast microscopy (DIC) and epifluorescence modalities using a Nikon Ti-E Perfect Focus inverted microscope equipped with a iXon+ DU897 EM Camera, either a 40× oil or a 100×/1.49 NA oil objective and an Intensilight System M lamp and 340–380 nm/500–550 nm excitation and emission filters, respectively, to detect probe 4 fluorescence, and 545–570 nm/578–625 nm emission and excitation filters, respectively, to detect DsRed fluorescence.

## RESULTS

Reported for the first time in the 1930s,<sup>56</sup> aryl fluorosulfates (the functional group in probes 3 and 4; recently studied more comprehensively<sup>45</sup>) have been reported in less than 20 publications and patents. The paucity of publications is likely due to the inconvenient synthetic methodology of the past,<sup>57,58</sup> as well as the perception that aryl fluorosulfates would be highly reactive and, therefore, incompatible with biological applications. However, as recently demonstrated by the Sharpless laboratory, the reactivity of the aryl fluorosulfate functional group is very low and vastly different from its chlorosulfate counterpart (ArOSO<sub>2</sub>Cl).<sup>45,58–60</sup> Aryl fluorosulfates can now easily be prepared from phenols via a reaction with the gas SO<sub>2</sub>F<sub>2</sub> (sulfuryl fluoride) under basic conditions (Et<sub>3</sub>N) in dichloromethane.<sup>45,61–63</sup> The resulting aryl fluorosulfates are typically produced in high yields and are remarkably stable, even at extremes of pH and temperature.<sup>45</sup> Moreover, aryl fluorosulfates are more stable toward acid–base catalyzed disruption at their S-(VI)-center than their deoxy relatives, i.e., aryl sulfonyl fluorides (ArSO<sub>2</sub>F).<sup>45</sup>

Consistent with the low reactivity of aryl fluorosulfates, the synthesis of candidate aryl fluorosulfate probe 4 commenced with the installation of the fluorosulfate functional group (95% yield) onto the structure of 4-hydroxybenzoic acid (5), employing SO<sub>2</sub>F<sub>2</sub> (sulfuryl fluoride) and Et<sub>3</sub>N in CH<sub>2</sub>Cl<sub>2</sub>/H<sub>2</sub>O (3:2)<sup>45,63</sup> (Figure 2B; and Supporting Information Experimental Methods). Subsequent acid chloride formation,

coupling with hydrazide (7), and TsCl-mediated oxadiazole ring formation led to 8. Demethylation in the presence of L-methionine in methanesulfonic acid then generated the desired aryl fluorosulfate probe 4 in 48% overall yield.<sup>25</sup> The same sequence of steps was used to prepare the *meta* analogue, candidate probe 3.

We first evaluated the ability of aryl sulfonyl fluoride 2, as well as aryl fluorosulfate probes 3 and 4, to bind to and/or bind to and react with wild-type TTR (TTR<sup>WT</sup>). Sulfonyl fluoride 1 served as a positive control for the covalent modification of TTR.<sup>25</sup> Probes 1–4 (7.2 μM) were individually incubated with recombinant TTR<sup>WT</sup> (3.6 μM) for 24 h (37 °C). The possibility of conjugate formation was monitored by liquid chromatography–mass spectrometry (LC-ESI-MS). The 2:1 ratio of small molecule to TTR<sup>WT</sup> was employed because each C<sub>2</sub>-symmetric tetramer has two small molecule binding sites (Figure 1A). Probe 4 reacted only very slowly with TTR<sup>WT</sup>. There was no detectable reaction after 1 h, which is the longest unicellular imaging period utilized in this manuscript (Figure S1 and S2). A 24 h incubation period was required to observe a 6% modification yield, equal to the incubation period used for *C. elegans* imaging in this manuscript. As only 2/4 subunits of TTR are modifiable, the theoretical maximal yield of modification is 50%.<sup>64</sup>

Surprisingly, the product detected by mass spectrometry was TTR<sup>WT</sup> covalently linked to a SO<sub>3</sub><sup>−</sup> functional group (mass of intact TTR<sup>WT</sup> monomer = 13 892 Da, modified TTR<sup>WT</sup> monomer = 13 972 Da) (Figures 2C, S1, S2, Table S1). Formation of the TTR-(CH<sub>2</sub>)<sub>4</sub>N(H)-SO<sub>2</sub>-OAr conjugate derived from probe 4 (Figure 2C) was not detected; however, its transient presence was inferred as a reactive intermediate hydrolyzed to afford TTR-SO<sub>3</sub><sup>−</sup>. We hypothesize that the hydrolysis of TTR-(CH<sub>2</sub>)<sub>4</sub>N(H)-SO<sub>2</sub>-OAr (Figure 2C) is somehow catalyzed by TTR<sup>WT</sup>, as we have not observed the hydrolysis of analogous conjugates.<sup>15,25</sup> The yield of TTR-SO<sub>3</sub><sup>−</sup> resulting from treatment of TTR<sup>WT</sup> by the *meta* probe 3 was higher, but still incomplete: 29% of TTR-SO<sub>3</sub><sup>−</sup> was formed after a 24 h incubation period (Figure S2, Table S1). Notably, the simultaneous presence of the TTR-(CH<sub>2</sub>)<sub>4</sub>N(H)-SO<sub>2</sub>-OAr conjugate derived from probe 3 (detected mass = 14 277 Da)

and the hydrolysis product TTR-(CH<sub>2</sub>)<sub>4</sub>N(H)-SO<sub>3</sub><sup>-</sup> was detected after 1, 2, and 4 h of incubation (Figures S1 and S2, Table S1), supporting the presence of the inferred intermediate during the slow reaction between TTR and probe 4. Further LC-MS-MS analysis of the reaction product formed from probe 3 reacting with TTR<sup>WT</sup> revealed modification of the Lys-15 residue (Figure S3).<sup>15,16,25</sup> No modification of the TTR<sup>K15A</sup> mutant tetramer was observed when the pK<sub>a</sub>-perturbed Lys-15 was replaced by Ala (Figure S4). The *meta* (1) and *para* (2) sulfonyl fluorides (Figure 2A), whose reaction with TTR<sup>WT</sup> led to the formation of stable TTR-ligand conjugates (Figures S1, S2, Table S1), exhibited an enhanced but analogous difference in reactivity toward TTR<sup>WT</sup>. The *meta* sulfonyl fluoride 1 nearly quantitatively modified TTR<sup>WT</sup> after 1 h of incubation (mass of labeled TTR<sup>WT</sup> monomer = 14 262 Da), as reported previously.<sup>25</sup> In contrast, complete modification of TTR<sup>WT</sup> by the *para* sulfonyl fluoride 2 was not achieved, even after a 24 h incubation period.

To garner insight into the difference in reactivity of the *meta* and *para* aryl fluorosulfate isomers 3 and 4 with TTR<sup>WT</sup>, crystal structures of the complexes and/or conjugation products were determined (1.25 and 1.35 Å resolution, respectively, see Table S2 for data collection and refinement statistics). Since the 2-fold symmetry axis ( $C_2$ ) runs through the T<sub>4</sub>-binding site of TTR (Y-axis; Figure 1A), the resulting electron density maps of ligands within the T<sub>4</sub>-binding sites represent an average of the opposing ligand orientations generated by the crystallographic 2-fold symmetry axis, which can often hamper the modeling of nonsymmetrical ligands.<sup>39</sup>

The Fo – Fc electron density omit maps of the products of the reaction between probe 3 and TTR<sup>WT</sup> allowed for clear placement of both the bis-phenol 9 (Figures S5 and S6) and the sulfamated Lys-15 residue comprising modified TTR<sup>WT</sup> (Figure 3A) resulting from hydrolysis of the initial reaction product shown in Figure 2C. The 3,5-dichloro-4-hydroxy aryl ring was found to occupy the inner binding subsite. The 3,5-dichloro substituents were placed into halogen binding pocket (HBP) 3/3', while the 4-hydroxy group formed a hydrogen bond with the Ser117/117' side chains at the base of the T<sub>4</sub>-binding-pocket (Figure 3A).

The Fo – Fc electron density omit maps of unreacted probe 4 bound to TTR<sup>WT</sup> revealed probe 4 could bind in both the “forward” and “reverse” binding orientations within the T<sub>4</sub>-binding pockets (Figures 3B, 3C and S7). While the overlapping core of probe 4 could be modeled into the observed Fo – Fc density, it was more difficult to model the flexible fluorosulfate group in the outer binding subsite, especially at low occupancy. In the forward binding orientation, the fluorosulfate group penetrated past the S117/117' residues into a cavity formed at the center of the TTR tetramer (Figure 3B). Since only one fluorosulfate group could physically occupy that cavity at a time, it appeared that one molecule of probe 4 bound to binding site 1 in the forward mode while the other probe 4 bound to binding site 2 in the reverse mode within the same tetramer (Figure S8). Thus, the 3,5-dichloro-4-hydroxy ring can occupy the outer binding subsite (Figure 3B) or the inner binding subsite (Figure 3C). Finally, the product of the very slow two-step reaction between probe 4 and TTR<sup>WT</sup> (Figure 2C)—the bis-phenol 10 resulting from hydrolysis—was observed to bind in the “reverse” orientation to sulfamated TTR based on the Fo – Fc electron density omit map (Figure 3D). Consequently, the 3,5-dichloro substituents were found to occupy the outer binding subsite HBP1/1', while the *para*

phenol group was oriented into the inner T<sub>4</sub>-binding pocket where it formed hydrogen bonds with S117/117' (Figure 3D). Thus, we conclude that bis-phenol 10 must have dissociated and then rebound in the opposite orientation post-hydrolysis.

We next examined the photophysical properties of the sulfonyl fluoride-based probes 1 and 2,<sup>25</sup> and aryl fluorosulfate-based probes 3 and 4 in the absence of TTR. First, excitation and emission spectra and the values of the extinction coefficients for probes 1, 2, 3 and 4 were determined in dichloromethane (Table S3, Figure S9A). While all probes were found to exhibit  $\lambda_{\text{ex max}}$  close to 300 nm, the value of  $\lambda_{\text{em max}}$  ranged from 364 nm for probe 4 to 401 nm for its sulfonyl fluoride analogue probe 2. Generally, sulfonyl fluorides were found to be characterized by lower extinction coefficients than their fluorosulfate counterparts. Probe 4 exhibited the extinction coefficient value of 25 000 [M<sup>-1</sup> cm<sup>-1</sup>] (Table S3). Next, the environment sensitivity of probes 2, 3 and 4 was tested. Importantly for the intended fluorogenic applications, the fluorescence signal of probes 2, 3 and 4 in aqueous solution could not be detected (Figure 4, also see Figure S9B and Table

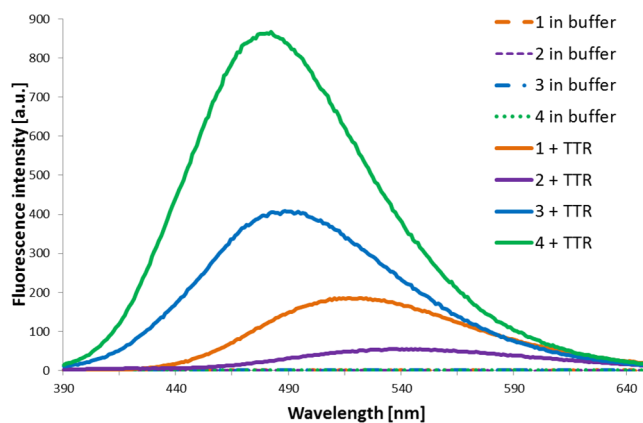


**Figure 4.** Fluorescence emission spectra of probes 1, 2, 3, and 4 (7.2  $\mu$ M) in buffer and bound to TTR<sup>WT</sup> (3.6  $\mu$ M) after 1 h incubation at 37 °C. Probe 1 forms a conjugate with TTR<sup>WT</sup> with 42% yield (max. modification is 50%) after a 1 h incubation period. Probe 2 forms a conjugate with TTR<sup>WT</sup> with 21% yield after a 1 h incubation period. Effectively, probe 3 and probe 4 do not react with TTR<sup>WT</sup> within 1 h.

S4 for a comparison of the effect of solvent polarity on fluorescence intensity, and excitation and emission wavelengths of probe 4). Incubation of probes 1, 2, and 3 (7.2  $\mu$ M) with recombinant TTR<sup>WT</sup> (3.6  $\mu$ M) for 1 h led to the formation of fluorescent conjugates in the cases of probes 1 and 2 (Figure 4 and Figures S2, S10, Table S5) or mostly a noncovalent fluorescent complex with probe 3 (Figures 4 and S2). Incubation of probe 4 (7.2  $\mu$ M;  $\lambda_{\text{ex max}} = 345$  nm,  $\lambda_{\text{em max}} = 481$ , Table S5) with TTR led to the formation of a fluorescent noncovalent complex (Figure 4), as demonstrated by a time dependent LC-ESI-MS analysis (Figure S1, S2, Table S1). Notably, the fluorescence intensity of the noncovalent complex between TTR<sup>WT</sup> and probe 4 (TTR·4; after 1 h of incubation) was five times higher than the fluorescence intensity of the previously reported TTR-sulfonyl fluoride 1 conjugate, and about 20 times higher than the emission from the TTR-sulfonyl fluoride 2 conjugate (Figure 4). The TTR·4 complex exhibited a higher fluorescence intensity than the analogous TTR·3 complex (small amount of conjugate formation; Figure 4;

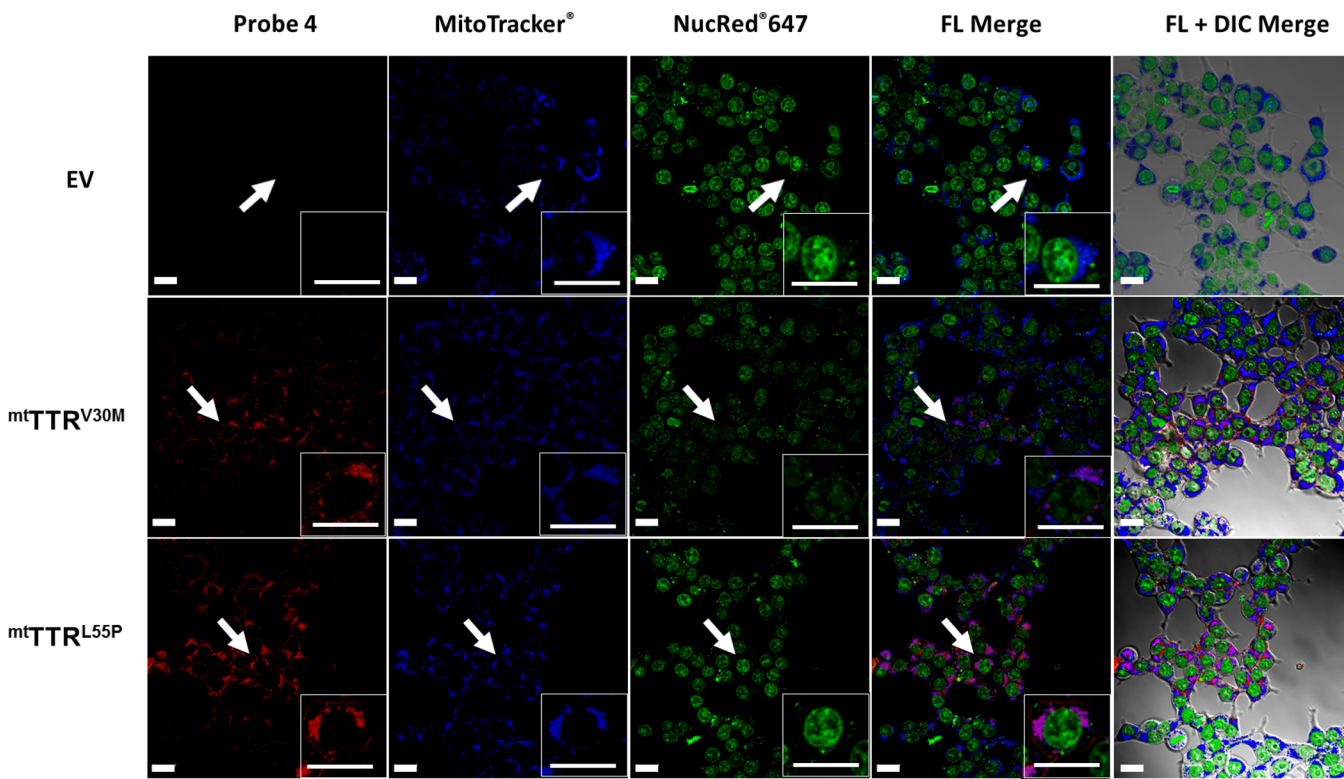


**Figure 5.** Confocal fluorescence microscopy images of living HEK293T cells transfected with an empty vector (EV; pcDNA3.1(+)) or  ${}^{\text{mt}}\text{TTR}^{\text{V30M}}$  or  ${}^{\text{mt}}\text{TTR}^{\text{L55P}}$  constructs, and treated with probe 4 (20  $\mu\text{M}$ ) for 20 min, followed by a 30 min incubation/diffusion period in probe-free media prior to imaging. Fluorescent image labels: probe 4 = red, mitochondrial stain - MitoTracker Orange = blue, nucleus stain - NucRed = green, FL Merge = fluorescence signal overlap, FL + DIC Merge = fluorescence and bright-field overlap. Scale bar = 20  $\mu\text{m}$ . Arrows indicate the cells shown at higher magnification in the insets. Identical microscope settings were used for acquisition of TTR-transfected and EV-transfected cell images.

$\lambda_{\text{ex max}} = 338 \text{ nm}$ ,  $\lambda_{\text{em max}} = 488 \text{ nm}$  for TTR·3 complex, Table S5).

Interestingly, extended incubation of probe 3 with recombinant TTR<sup>WT</sup> led to noticeable changes in the fluorescence emission spectra, likely because of the Lys15- $\epsilon\text{NH}-\text{SO}_3^-$  sulfamate contribution (29% sulfamation after 24 h of incubation) and the linked contribution from binding of the bis-phenol 9 (Figure 3A, S11A, S11B, Table S5). In contrast, the TTR·4 noncovalent complex dominated the fluorescence spectrum, even after 24 h (Figure S11C, S11D, Table S5), despite  $\leq 6\%$  sulfamation (Figure S2), indicating that the solvatochromic fluorescence enhancement is more significant than the reactivity-based turn-on, unlike the situation with sulfonyl fluorides.<sup>25</sup>

We next assessed the applicability of probe 4 for TTR imaging in living cells by examining the ability of probe 4 to bind to TTR tetramers localized to different subcellular compartments, including mitochondria. It is very challenging to deliver nonlipophilic cation probes or drug-like molecules into mitochondria, as reflected by the limited number of nonlipophilic cation small molecules that successfully target this organelle, despite its connection to a variety of diseases.<sup>65,66</sup> The established paradigm for creating mitoactive small molecule probes requires the attachment of a large, lipophilic cation to a substructure targeting a mitochondrial POI, which results in the accumulation of these small molecules inside mitochondria as a consequence of the mitochondrion's large, negative electrochemical cross-membrane potential.<sup>67,68</sup> Probe 4 lacks this consensus feature. To evaluate the capacity of probe 4 to image TTR targeted to mitochondria, we prepared TTRs

targeted to mitochondria by a COXVIII mitochondrial targeting sequence, similar to the approach previously described for a monomeric TTR variant ( ${}^{\text{mt}}\text{M-TTR}^{\text{WT}}$ ).<sup>69</sup> For these experiments, we used the destabilized TTR variants L55P and V30M, since these variants are more efficiently imported and retained in mitochondria. This was shown by the processing of the N-terminal targeting sequence, as analyzed by immunoblot analysis (Figures S12A and S13A). In contrast, the more stable wild-type  ${}^{\text{mt}}\text{TTR}^{\text{WT}}$  accumulated both in the cytosol and mitochondria (Figures S12A and B), presumably due to its stable tetramerization interfering with mitochondrial import. As shown in Figure S14, probe 4 created equivalently bright fluorescent complexes with tetrameric recombinant TTR<sup>V30M</sup> and TTR<sup>WT</sup> in vitro, whereas the fluorescence intensity of the TTR<sup>L55P</sup>·4 tetramer was slightly lower in buffer. Thus, probe 4 should be efficient at detecting intracellular levels of these mutants.

The subcellular localization of  ${}^{\text{mt}}\text{TTR}^{\text{L55P}}$  and  ${}^{\text{mt}}\text{TTR}^{\text{V30M}}$  in HEK293T cells was analyzed using confocal microscopy. Transfected cells were incubated with media containing probe 4 (20  $\mu\text{M}$ ) for 20 min at 37 °C. Simultaneous treatment with MitoTracker Orange and NucRed in the same media allowed parallel visualization of mitochondria and nuclei, respectively (Figure 5). The media was removed and the cells were incubated for 30 min in probe-free media. In cells expressing  ${}^{\text{mt}}\text{TTR}^{\text{L55P}}$  or  ${}^{\text{mt}}\text{TTR}^{\text{V30M}}$  treated with probe 4, fluorescence from the TTR·4 complex colocalized with a mitochondrial marker (Figure 5). No fluorescence was observed in empty vector (EV)-transfected control cells treated with probe 4. The images in Figure 5 constitute the first evidence for the ability of

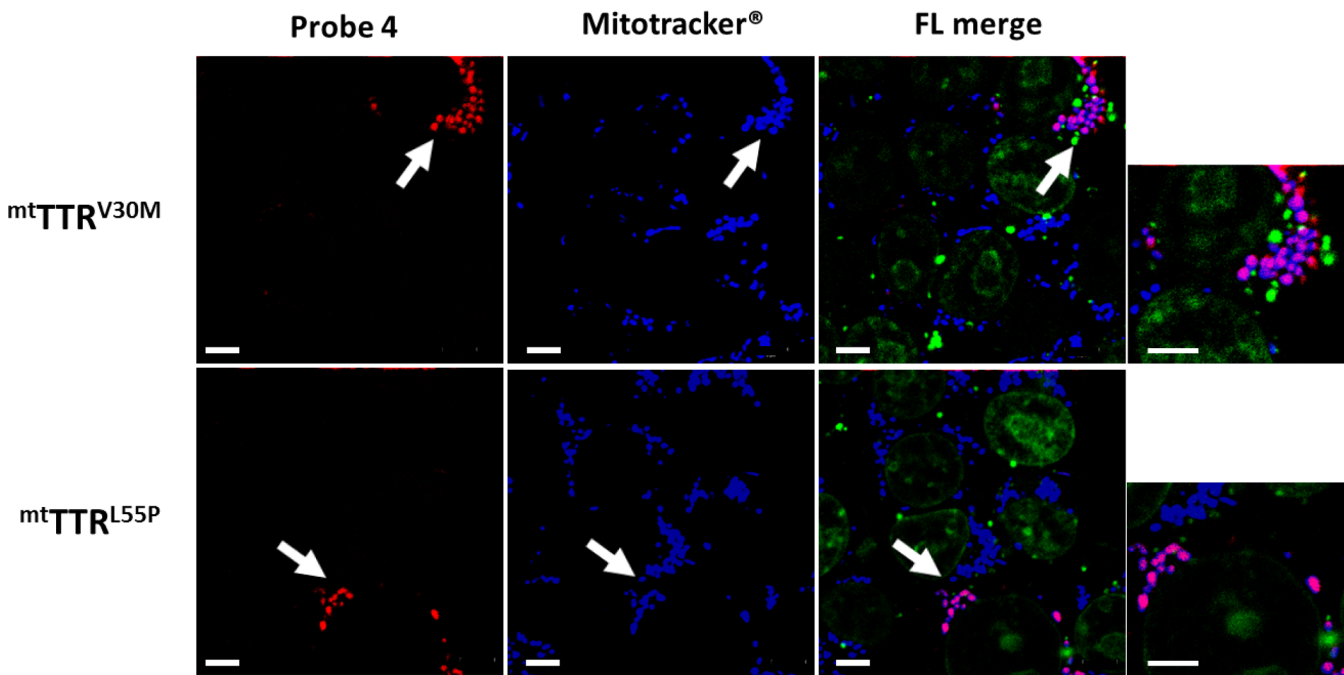


**Figure 6.** Confocal fluorescence microscopy images of living HEK293T cells transfected with  $^{mt}\text{TTR}^{\text{V30M}}$  or  $^{mt}\text{TTR}^{\text{L55P}}$  constructs, and treated with probe 4 (5  $\mu\text{M}$ ) for 30 s, followed by a 10 min incubation/diffusion period in probe-free media prior to imaging. Fluorescent images labels: probe 4 = red, mitochondrial stain - MitoTracker Orange = blue, nucleus stain - NucRed = green, FL Merge = fluorescence signal overlap. Scale bar = 5  $\mu\text{m}$ . Arrows indicate the cells shown at higher magnification (far right panels).

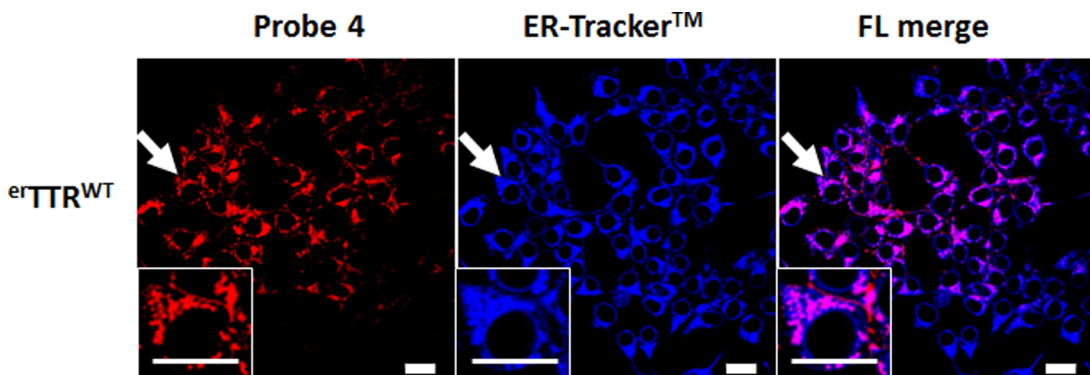


**Figure 7.** Confocal fluorescence microscopy images of living HEK293T cells transfected with  $^{er}\text{TTR}^{\text{WT}}$  construct and treated with probe 4 (5  $\mu\text{M}$ ) for 30 s, followed by a 15 min incubation/diffusion period in probe-free media. Fluorescent image labels: probe 4 = red, ER stain - ER-Tracker Red = blue, FL Merge = fluorescence signal overlap. Scale bar = 20  $\mu\text{m}$ . Arrows indicate the cells shown at higher magnification in the insets.

probe 4 to selectively label TTR localized to the mitochondria of living cells. In contrast and for unknown reasons, probe 3 was found to colocalize to a lesser extent with mitochondria, and fluorescence was detected in what are likely non-mitochondrial subcellular compartments (Figure S15).

To further examine the selectivity of aryl fluorosulfates 3 and 4 in the context of the human cellular proteome, HEK293T cells transfected with  $^{mt}\text{TTR}^{\text{L55P}}$  variant or control cells lacking variant TTR expression were incubated with probes 3 or 4 (100  $\mu\text{M}$ ) for 1 or 6 h (37 °C). Native gel analysis revealed TTR binding and fluorescence in lysates of cells transfected with  $^{mt}\text{TTR}^{\text{L55P}}$ , comparable to recombinant TTR<sup>WT</sup> preincubated with each probe (Figure S16A and S16B). TTR was not detected by probe 3 or probe 4 in control samples lacking TTR overexpression, indicating that these cells either lack or have

very low levels of endogenous TTR passing through the secretory pathway. Even though off-target labeling could be observed for probes 3 and 4, both aryl fluorosulfates were found to be generally unreactive toward the proteome. No noticeable changes in the degree of labeling could be observed when comparing 1 to 6 h (Figure S16A and S16B). Importantly, the small molecule treatment period in these experiments was conducted on a time scale four to 20 times longer than the fluorescence-based cellular imaging time scale discussed below.

Next, to test the sensitivity of probe 4, we further optimized the conditions for the detection of TTR variants in mitochondria in terms of the treatment period (Figure S17), the post-treatment probe-free incubation period (Figure S18), and the probe 4 concentration (Figure S19). Clear detection of

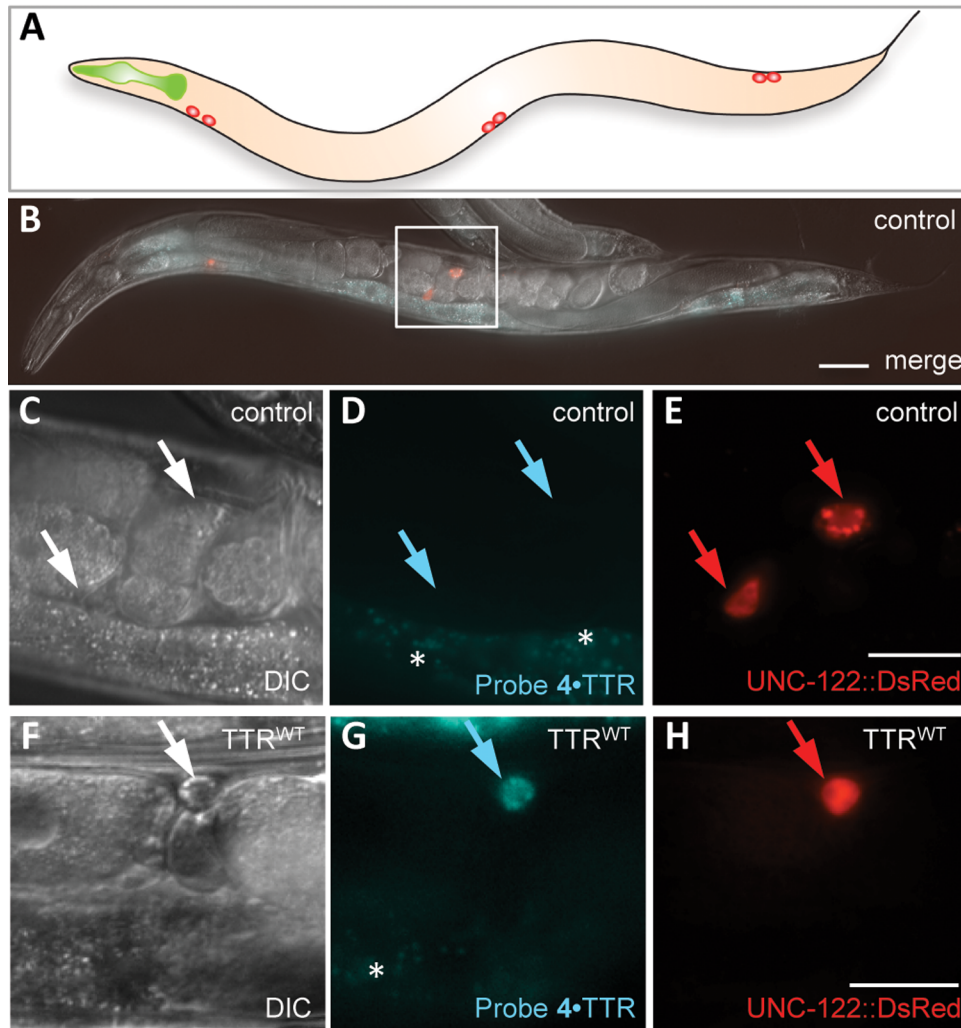


**Figure 8.** *In vivo* labeling of TTR<sup>WT</sup> in coelomocytes of *C. elegans* with probe 4. (A) Schematic of a *C. elegans* worm showing the position of the six coelomocytes in red. The pharynx is shown in green. (B) Merged Nomarski differential interference contrast (DIC) photomicrograph and fluorescent images of a probe 4-treated control (*rol-6*) day 2 adult worm. All fluorescent images have the following labels: red = UNC-122::DsRed-labeled coelomocytes (3 are seen in this focal plane); cyan = probe 4. Scale bar = 50  $\mu$ m. (C–E) Enlargement images of boxed region of the same worm shown in B. Arrows point to two coelomocytes in the focal plane. Scale bar = 25  $\mu$ m. (F–H) Enlargement images of a day 2 old worm expressing TTR<sup>WT</sup> treated with probe 4. Arrow points to a coelomocyte in the focal plane. Scale bar = 25  $\mu$ m. Asterisks denote unspecific gut autofluorescence, observed in untreated *C. elegans*, as well as in *C. elegans* treated with probe 4; see Figure S20. Identical microscope settings were used for acquisition of control and TTR transgenic worm images.

mitochondrial TTR using probe 4 was achieved by treating live cells with a 5  $\mu$ M concentration of probe 4 for 30 s, followed by a post-treatment probe-free incubation period of 10–15 min in media. The accumulation of <sup>mt</sup>TTR<sup>V30M</sup> and <sup>mt</sup>TTR<sup>L55P</sup> in the mitochondria imaged by probe 4 using these conditions is clear (Figure 6). Expression of endoplasmic reticulum (ER)-targeted TTR (<sup>er</sup>TTR<sup>WT</sup>) in the secretory pathway of HEK293T cells also enabled facile imaging of TTR in the ER (Figures 7 and S13B).

Finally, to further demonstrate the applicability of probe 4 for imaging the location of TTR in a living multicellular organism, we treated *C. elegans* expressing human TTR<sup>WT</sup> in the body wall muscle under the *unc-54p* body wall muscle promoter (*him-5*; *unc-54p::hTTR(WT)* + *rol-6*)<sup>70</sup> with probe 4 (10  $\mu$ M). Control (*rol-6*) worms lacking TTR<sup>WT</sup> expression were also treated with probe 4 (10  $\mu$ M). In both the TTR transgenic and in the control worms, probe 4 was applied overnight to the medium of day 1 old adult *C. elegans* grown in

liquid culture in 96-well plates.<sup>55,71</sup> The day 2 old adult worms pretreated with probe 4 were then placed on agarose pads and imaged using epifluorescence microscopy after *C. elegans* immobilization with sodium azide.<sup>72</sup> We imaged within a 24 hour period from treatment because less than 6% covalent modification of TTR by probe 4 was observed after 24 h *in vitro* (Figure S2 and Table S1), an extent of reaction that does not alter the observed fluorescence emission spectra (Figure S11D). We detected probe 4 fluorescence specifically in six distinct cells that resembled coelomocytes, macrophage-like scavenger cells in the body cavity (pseudocoelom) of the worm that are highly active in endocytosis and degradation of soluble molecules (Figure 8).<sup>73</sup> To test whether probe 4 localized to coelomocytes, we visualized coelomocytes in probe 4-treated TTR<sup>WT</sup> and control worms expressing a fluorescent tag under the *unc-122* promoter (UNC-122::DsRed), which is expressed in all coelomocytes.<sup>74</sup> The TTR-4 complex colocalized with

UNC-122::DsRed in all six coelomocytes in TTR<sup>WT</sup> ( $n = 19/21$ ), but not in control animals ( $n = 0/11$ ; Figures 8, S20).

The amount of TTR secreted from a mammalian cell has been shown to be modestly increased ( $\approx 20\%$ ) if high concentrations of a small molecule TTR probe is incubated with the cells for a period exceeding the half-life of TTR secretion ( $\approx 4$  h from eukaryotic cells) owing to pharmacologic chaperoning.<sup>75</sup> Pharmacologic chaperoning results when a small molecule binds to the TTR tetramer in the endoplasmic reticulum, shifting the folding equilibrium at the expense of endoplasmic reticulum-associated degradation. Thus, we hypothesize that pharmacologic chaperoning by probe 4 will dose-dependently and modestly increase the amount of TTR secreted by *C. elegans* over the overnight preimaging period utilized in this paper. This is not a consideration in the cell-based experiments presented above, which are completed in  $<1$  h.

## ■ DISCUSSION

In our quest to develop new fluorogenic probes for studying TTR, we decided to evaluate the photophysical parameters and reactivity of fluorosulfate probes.<sup>45</sup> This effort revealed that fluorosulfates are suitable functional groups to replace more traditional electron-withdrawing groups in solvatochromic fluorophores. For our purpose, we utilized 2,5-diphenyl-1,3,4-oxadiazole-based chromophores, which due to their photophysical properties, and thermal and chemical stability, have been widely applied in the development of optical materials, e.g., OLEDs, and fluorophores.<sup>76–79</sup> Many 1,3,4-oxadiazoles have been developed for applications in medicinal chemistry.<sup>80</sup> However, to the best of our knowledge, probes 1–4 and their analogues reported previously, are the only examples of fluorogenic probes targeting a specific POI.<sup>25</sup>

In particular, probe 4 is an environment-sensitive fluorophore whose emission is very low in aqueous buffers, but is restored upon binding to TTR. In comparison to the previously reported sulfonyl fluoride probe 1, which forms a conjugate with TTR, noncovalent binding of probe 4 to TTR exhibited blue-shifted excitation and emission maxima ( $\lambda_{\text{ex max}} = 345$  nm and  $\lambda_{\text{em max}} = 481$  nm vs  $\lambda_{\text{ex max}} = 365$  nm and  $\lambda_{\text{em max}} = 520$  nm for the TTR-1 conjugate), and higher quantum yield upon formation of a probe 4-TTR<sup>WT</sup> complex (0.44 vs 0.19 for the TTR-1 conjugate). We showed that probe 4 could be used as a subcellular marker to detect TTR localization in living cells (Figures 6 and 7). To the best of our knowledge, probe 4 is the first example of a fluorogenic small molecule meeting the Lipinski rule of five criteria that selectively targets a POI inside the mitochondrial matrix.<sup>81</sup> Because of its excellent cell permeability, time-lapse imaging (Figure S18) revealed that aryl fluorosulfate 4 undergoes very fast diffusion across various membranes before accumulating in the compartment of the cell containing TTR. First, probe 4 bound to the hydrophobic plasma membrane, as well as the ER and mitochondrial membranes, which restored the fluorescence of probe 4 that is dark in aqueous solution. Within 15 min, probe 4 localized to the compartment harboring TTR (Figure S18).

While probe 4 was found to form a noncovalent complex with TTR<sup>WT</sup> on the time scale of the imaging experiments, extended treatment of TTR<sup>WT</sup> with probe 4 (24 h) led to TTR<sup>WT</sup> sulfamation (6%, Table S1). Our data suggest that sulfamated TTR (TTR-(CH<sub>2</sub>)<sub>4</sub>N(H)-SO<sub>3</sub><sup>-</sup>) is generated in a two-step reaction, consisting of the initial nucleophilic attack by the pK<sub>a</sub>-perturbed Lys-15 ε-amino group on the fluorosulfate S

atom, resulting in the displacement of the fluorine atom, a reaction apparently catalyzed by TTR binding and activation of the normally unreactive fluorosulfate functional group (Figure 2C).<sup>45</sup> We hypothesize that fluorosulfate activation could result from hydrogen bond formation between the fluorine atom and a TTR residue within the T<sub>4</sub>-binding pocket<sup>82–84</sup> or via interfacial or electric field effects.<sup>85</sup> Formation of the conjugate (TTR-(CH<sub>2</sub>)<sub>4</sub>N(H)-SO<sub>2</sub>-OAr) was then followed by a relatively rapid hydrolysis step, apparently catalyzed by TTR, where the activated water molecule attacked the S atom, affording a noncovalently bound phenol and TTR sulfamated on the Lys-15 ε-amino group, i.e., TTR-(CH<sub>2</sub>)<sub>4</sub>N(H)SO<sub>3</sub><sup>-</sup> (Figure 2C).

We believe that the hydrolytic reactivity of TTR-(CH<sub>2</sub>)<sub>4</sub>-NH-SO<sub>2</sub>-OAr is a special case. For most proteins, we hypothesize that this adduct will be resistant to hydrolysis,<sup>45</sup> but this remains to be proven. Irreversible protein modification through functional group transfer has been reported previously, e.g., the aspirin-mediated inhibition of COX enzymes results from transfer of an acetyl group onto a serine residue.<sup>86–88</sup> The effect of sulfamation on TTR properties remains to be elucidated, as probes 3 and 4 were found to stabilize TTR structure and prevent fibril formation independently from the degree of covalent modification, as measured by the previously reported acid-induced fibril formation assay (Figure S21, S22).<sup>42,89–91</sup>

It is unclear at this juncture whether the generally lower reactivity of the fluorosulfates relative to the sulfonyl fluorides (Figure 2A) results from a nonoptimal reaction geometry owing to the extra oxygen atom in the fluorosulfates, the lower inherent reactivity of fluorosulfates vs sulfonyl fluorides (the most likely explanation), or both. Another possible contributor to the observed differences in reactivity of probes 1–4 may derive from distinctions in their TTR binding cooperativity. Probe binding to the two T<sub>4</sub>-binding sites TTR, can be negatively cooperative, noncooperative or positively cooperative,<sup>91</sup> likely due to conformational changes within TTR. Isothermal titration calorimetry revealed that probe 4 (non-covalent binder on the time scale of the experiments) bound to TTR<sup>WT</sup> with negative cooperativity ( $K_{d1} = 2$  nM and  $K_{d2} = 719$  nM, Figure S23).

Fluorescent small molecule ligands have proven to be valuable for a variety of applications.<sup>92,93</sup> The next generation of fluorophores, i.e., fluorogenic probes that only exhibit fluorescence upon binding the POI in the context of a complex biological environment, are gaining in popularity as they eliminate the need for additional washout steps to reduce the high fluorescence background typically resulting from the presence of unreacted or nonspecifically bound permanently fluorescent small molecules. Additionally, application of fluorogenic protein-selective probes excludes the need to attach an inherently fluorescent protein or small molecule-based fluorescent protein tag to the POI. Herein, we demonstrate that fluorogenic probe 4 can detect and localize overexpressed TTR within mammalian cells and in living *C. elegans*. Previous fluorogenic molecules have been used for detection of phosphatases in cells and in *Drosophila* brains,<sup>24</sup> but these studies required the delivery of the fluorogenic probes into cells with cell-penetrating peptides. The advantage of probe 4 is that it can be efficiently delivered into cells and cellular organelles, without the need to append a membrane-penetrating substructure to the fluorophore. In addition, the selectivity of probe 4 to bind to the folded TTR tetramer allows the

distinction of this TTR conformer over other conformations lacking a probe 4 binding site, such as misfolded TTR or TTR aggregates. The use of fluorogenic probes in living systems could provide invaluable insights into the kinetics of TTR secretion and degradation, and how these processes could be modulated therapeutically to ameliorate the TTR amyloidoses.

## CONCLUSION AND PERSPECTIVE

In summary, the data presented herein validate the use of the noncovalent, fluorogenic, small molecule aryl fluorosulfate probe **4** for the imaging of properly folded TTR within organelles in living cells. Moreover, probe **4** detected TTR in six macrophage-like cells in the multicellular organism *C. elegans*. Creating high affinity ( $K_{d1} = 2$  nM), selective fluorogenic probes for TTR is part of a broader effort by many researchers to discover what one hopes will ultimately be more generalizable methods for the labeling of individual proteins with fluorogenic probes. Although, probe **4** exhibited very slow reactivity toward TTR, it is a noncovalent probe with regard to the time scale of the imaging experiments performed herein. Probe **4** rapidly and efficiently penetrated cell and organelle membranes. Binding-associated activation of probe **3** and probe **4** by TTR seems to be a necessary requirement for TTR conjugation and likely for the modification of other proteins by aryl fluorosulfates, as evidenced by the general lack of reactivity of these probes with more than a few members of the proteome in living cells.

## ASSOCIATED CONTENT

### Supporting Information

Supplementary Tables, Figures, Experimental Details and Synthetic Methods are supplied as Supporting Information. The Supporting Information is available free of charge on the ACS Publications website at DOI: 10.1021/jacs.5b03042.

## AUTHOR INFORMATION

### Corresponding Authors

\*encalada@scripps.edu  
\*jkelly@scripps.edu

### Present Address

<sup>¶</sup>aTyr Pharma, 3545 John Hopkins Court, Suite 250, San Diego, California 92121, United States.

### Notes

The authors declare no competing financial interest.

## ACKNOWLEDGMENTS

We acknowledge NIH Grants DK046335 (J.W.K.), DK075295 (J.W.K. and R.L.W.), GM100934 (L.N.), and AI42266 (I.A.W.), the Skaggs Institute for Chemical Biology, The Ellison Medical Foundation (R.L.W. and S.E.E.), Arlene and Arnold Goldstein (S.E.E.), and the Lita Annenberg Hazen Foundation (J.W.K.) for financial support. E.R.G. is supported by the George E. Hewitt Foundation for Medical Research. J.C.G. was supported by the NIH (F32-HL099245) and is currently supported by an American Heart Association fellowship. Y.S.E. is supported by a German Academic Exchange Service (DAAD) postdoctoral fellowship. Portions of this research were carried out at the Stanford Synchrotron Radiation Lightsource, a Directorate of SLAC National Accelerator Laboratory and an Office of Science User Facility operated for the U.S. Department of Energy Office of Science by Stanford University. The SSRL Structural Molecular Biology

Program is supported by the DOE Office of Biological and Environmental Research and by the National Institutes of Health, National Institute of General Medical Sciences (including P41GM103393) and the National Center for Research Resources (P41RR001209). We thank Chris Link (University of Colorado), and Cori Bargmann (Rockefeller University), and the *Caenorhabditis* Genetics Center (CGC) for *C. elegans* strains. We are grateful to Colleen Fearn for carefully reading and editing the manuscript.

## REFERENCES

- (1) Crivat, G.; Taraska, J. W. *Trends Biotechnol.* **2012**, *30*, 8.
- (2) Jing, C.; Cornish, V. W. *Acc. Chem. Res.* **2011**, *44*, 784.
- (3) Newman, R. H.; Fosbrink, M.; Zhang, J. *Chem. Rev.* **2011**, *111*, 3614.
- (4) Van, T. N. N.; Morris, M. C. *Prog. Mol. Biol. Transl. Sci.* **2013**, *113*, 217.
- (5) Adams, S. R.; Tsien, R. Y. *Nat. Protoc.* **2008**, *3*, 1527.
- (6) Soh, N. *Sensors* **2008**, *8*, 1004.
- (7) Sun, X.; Zhang, A.; Baker, B.; Sun, L.; Howard, A.; Buswell, J.; Maurel, D.; Masharina, A.; Johnsson, K.; Noren, Ch.J.; Xu, M. Q.; Correa, I. R. *ChemBioChem* **2011**, *12*, 2217.
- (8) Nadler, A.; Schultz, C. *Angew. Chem., Int. Ed.* **2013**, *52*, 2408.
- (9) Mizukami, S.; Hori, Y.; Kikuchi, K. *Acc. Chem. Res.* **2013**, *47*, 247.
- (10) Karpenko, I. A.; Kreder, R.; Valenica, Ch.; Villa, P.; Mendre, Ch.; Mouillac, B.; ly, Y. M.; Hibert, M.; Bonnet, D.; Klymchenko, A. S. *ChemBioChem* **2014**, *15*.
- (11) Xing, B.; Khanamiryan, A.; Rao, J. *J. Am. Chem. Soc.* **2005**, *127*, 4158.
- (12) Zhang, H.; Fan, J.; Wang, J.; Zhang, S.; Dou, B.; Peng, X. *J. Am. Chem. Soc.* **2013**, *135*, 11663–11669.
- (13) Lukinavici, G.; R, L.; Deste, E.; Masharina, A.; Göttfert, F.; Ta, H.; Güther, A.; Fournier, M.; Rizzo, S.; Waldmann, H.; Blaukopf, C.; Sommer, C.; Gerlich, D. W.; Arndt, H. D.; Hell, S. W.; Johnsson, K. *Nat. Methods* **2014**, *11*, 731.
- (14) Han, J.; Han, M. S.; Tung, C. H. *Mol. BioSyst.* **2013**, *9*, 3001.
- (15) Choi, S.; Ong, D. S. T.; Kelly, J. W. *J. Am. Chem. Soc.* **2010**, *132*, 16043.
- (16) Suh, E. H.; Liu, Y.; Connelly, S.; Genereux, J. C.; Wilson, I. A.; Kelly, J. W. *J. Am. Chem. Soc.* **2013**, *135*, 17869.
- (17) Liu, Y.; Tan, Y. L.; Zhang, X.; Bhabha, G.; Ekiert, D. C.; Genereux, J. C.; Cho, Y.; Kipnis, Y.; Bjelic, S.; Baker, D.; Kelly, J. W. *Proc. Natl. Acad. Sci. U. S. A.* **2014**, *111*, 4449.
- (18) Grimm, J. B. H.; L, M.; Lavis, L. D. *Prog. Mol. Biol. Transl. Sci.* **2013**, *113*, 1.
- (19) Shibata, A.; Nakano, Y.; Ito, M.; Araki, M.; Zhang, J.; Yoshida, Y.; Shuto, S.; Mannervik, B.; Mogenstern, R.; Ito, Y.; Abe, H. *Analyst* **2013**, *138*, 7326.
- (20) Baba, R.; Hori, Y.; Mizukami, S.; Kikuchi, K. *J. Am. Chem. Soc.* **2012**, *134*, 14310.
- (21) Smith, E. L.; Bertozzi, C. R.; Beatty, K. E. *ChemBioChem* **2014**, *15*, 1101.
- (22) Sanchini, S.; Perruccio, F.; Piuzzi, G. *ChemBioChem* **2014**, *15*, 961.
- (23) Froemming, M. K.; Sames, D. *J. Am. Chem. Soc.* **2007**, *128*, 14518.
- (24) Li, L.; Ge, J.; Wu, H.; Xu, Q. H.; Yao, S. Q. *J. Am. Chem. Soc.* **2012**, *134*, 12157.
- (25) Grimster, N. P.; Connelly, S.; Baranczak, A.; Dong, J.; Krasnova, L. B.; Sharpless, K. B.; Powers, E. T.; Wilson, I. A.; Kelly, J. W. *J. Am. Chem. Soc.* **2013**, *135*, 5656.
- (26) Lang, K.; Davis, L.; Wallace, S.; Mahesh, M.; Cox, D. J.; Blackman, M. L.; Fox, J. M.; Chin, J. W. *J. Am. Chem. Soc.* **2012**, *134*, 10317.
- (27) Zhuang, Y. D.; Chiang, P. Y.; Wang, C. W.; Tan, K. T. *Angew. Chem., Int. Ed.* **2013**, *52*, 8124.
- (28) Shieh, P.; Hangauer, M. J.; Bertozzi, C. R. *J. Am. Chem. Soc.* **2012**, *134*, 17428.

- (29) Kamber, D. N.; Nazarova, L. A.; Liang, Y.; Lopez, S. A.; Patterson, D. M.; Shih, H. W.; Houk, K. N.; Prescher, J. A. *J. Am. Chem. Soc.* **2013**, *135*, 13680.
- (30) Speight, L. C.; Samanta, M.; Petersson, E. *J. Aust. J. Chem.* **2014**, *67*, 686.
- (31) Baranczak, A.; Connelly, S.; Liu, Y.; Choi, S.; Grimster, N. P.; Powers, E. T.; Wilson, I. A.; Kelly, J. W. *Biopolymers* **2014**, *101*, 484.
- (32) Li, X.; Gao, X.; Shi, W.; Ma, H. *Chem. Rev.* **2014**, *114*, 590.
- (33) Loving, G. S.; Sainlos, M.; Imperiali, B. *Trends Biotechnol.* **2009**, *28*, 73.
- (34) Klymchenko, A.; Mely, Y. *Prog. Mol. Biol. Transl. Sci.* **2013**, *113*, 35.
- (35) Wiseman, R. L.; Powers, E. T.; Kelly, J. W. *Biochemistry* **2005**, *44*, 16612.
- (36) Schreiber, G.; Richardson, S. J. *Comp. Biochem. Physiol., Part B: Biochem. Mol. Biol.* **1997**, *116*, 137.
- (37) Monaco, H. L.; Rizzi, M.; Coda, A. *Science* **1995**, *268*, 1039.
- (38) Hammarstrom, P.; Wiseman, R. L.; Powers, E. T.; Kelly, J. W. *Science* **2003**, *299*, 713.
- (39) Wojtczak, A.; Cody, V.; Luft, J. R.; Pangborn, W. *Acta Crystallogr., Sect. D: Biol. Crystallogr.* **1996**, *52*, 758.
- (40) Rappley, I.; Monteiro, C.; Novais, M.; Baranczak, A.; Solis, G.; Wiseman, R. L.; Helmke, S.; Maurer, M. S.; Coelho, T.; Powers, E. T.; Kelly, J. W. *Biochemistry* **2014**, *53*, 1993.
- (41) Berk, J. L.; Suhr, O. B.; Obici, L.; Sekijima, Y.; Zeldenrust, S. R.; Yamashita, T.; Hennegan, M. A.; Gorevic, P. D.; Litchy, W. J.; Wiseman, J. F.; Nordh, E.; Corato, M.; Lozza, A.; Cortese, A.; Robinson-Papp, J.; Colton, T.; Rybin, D. V.; Bisbee, A. B.; Ando, Y.; Ikeda, S.; Seldin, D. C.; Merlini, G.; Skinner, M.; Kelly, J. W.; Dyck, P. J. *J. Am. Med. Assoc.* **2013**, *310*, 2658.
- (42) Bulawa, C. E.; Connelly, S.; DeVit, M.; Wang, L.; Weigel, C.; Fleming, J. A.; Packman, J.; Powers, E. T.; Wiseman, R. L.; Foss, T. R.; Wilson, I. A.; Kelly, J. W.; Labaudiniere, R. *Proc. Natl. Acad. Sci. U. S. A.* **2012**, *109*, 9629.
- (43) Coelho, T.; Maia, L. F.; Martins, D. S. A.; Waddington, C. M.; Plante-Bordeneuve, V.; Lozeron, P.; Suhr, O. B.; Campistol, J. M.; Conceicao, I. M.; Schmidt, H. H. J.; Trigo, P.; Kelly, J. W.; Labaudiniere, R.; Chan, J.; Packman, J.; Wilson, A.; Grogan, D. R.; Imventarza, O. C.; Wainberg, P. J.; Berra, L. M.; Maultasch, H.; Gold, J.; Bardera, J. C. P.; Zibert, A. *Neurology* **2012**, *79*, 785.
- (44) Coelho, T.; Maia, L. F.; da Silva, A. M.; Cruz, M. W.; Plante-Bordeneuve, V.; Suhr, O. B.; Conceicao, I.; Schmidt, H. H.; Trigo, P.; Kelly, J. W.; Labaudiniere, R.; Chan, J.; Packman, J.; Grogan, D. R. *J. Neurol.* **2013**, *260*, 2802.
- (45) Dong, J.; Krasnova, L.; Finn, M. G.; Sharpless, K. B. *Angew. Chem., Int. Ed.* **2014**, *53*, 2.
- (46) Otwinowski, Z.; Minor, W. *Methods Enzymol.* **1997**, *276*, 307.
- (47) Emsley, P.; Cowtan, K. *Acta Crystallogr., Sect. D: Biol. Crystallogr.* **2004**, *60*, 2126.
- (48) Murshudov, G. N.; Skubák, P.; Lebedev, A. A.; Pannu, N. S.; Steiner, R. A.; Nicholls, R. A.; Winn, M. D.; Long, F.; Vagin, A. A. *Acta Crystallogr., Sect. D: Biol. Crystallogr.* **2011**, *67*, 355.
- (49) Lebedev, A. A.; Young, P.; Isupov, M. N.; Moroz, O. V.; Vagin, A. A.; Murshudov, G. N. *Acta Crystallogr., Sect. D: Biol. Crystallogr.* **2012**, *68*, 431.
- (50) Lovell, S. C.; Davis, I. W.; Arendall, W. B., 3rd; de Bakker, P. I.; Word, J. M.; Prisant, M. G.; Richardson, J. S.; Richardson, D. C. *Proteins* **2003**, *50*, 437.
- (51) Vriend, G. *J. Mol. Graphics* **1990**, *8*, 52.
- (52) Terwilliger, T. C. *Acta Crystallogr., Sect. D: Biol. Crystallogr.* **2003**, *59*, 38.
- (53) Brenner, S. *Genetics* **1974**, *77*, 71.
- (54) Mello, C.; Fire, A. *Methods Cell Biol.* **1995**, *48*, 451.
- (55) Solis, G. M.; Petrascheck, M. *J. Visualized Exp.* **2011**, *49*, 2496.
- (56) Lange, W.; Muller, E. *Chem. Ber.* **1930**, *63*, 2653.
- (57) Stevens, T. E. *J. Org. Chem.* **1968**, *33*, 2664.
- (58) Roth, G. P.; Fuller, C. E. *J. Org. Chem.* **1991**, *56*, 3493.
- (59) Hedayatullah, M.; Hugueny, J. C.; Guy, A. J. *Heterocycl. Chem.* **1984**, *21*, 1385.
- (60) Roth, G. I.; Thomas, J. A. *Tetrahedron Lett.* **1992**, *33*, 1959.
- (61) Hedayatullah, M.; Guy, A.; Denivelle, L. *C. R. Seances Acad. Sci., Vie Acad.* **1974**, *278*, 57.
- (62) Hedayatullah, M.; Guy, A.; Denivelle, L. *Phosphorus, Sulfur Silicon Relat. Elem.* **1980**, *8*, 125.
- (63) Ishii, A.; Ishimaru, T.; Yamazaki, T.; Yasumoto, M. WO 2013002040, 2013.
- (64) Choi, S.; Connelly, S.; Reixach, N.; Wilson, I. A.; Kelly, J. W. *Nat. Chem. Biol.* **2010**, *6*, 133.
- (65) Murphy, M. P. *Curr. Opin. Invest. Drugs* **2009**, *10*, 1022.
- (66) Shapira, A. H. V. *Lancet* **2012**, *379*, 1825.
- (67) Yousif, L. F.; Stewart, K. M.; Kelley, S. O. *ChemBioChem* **2009**, *10*, 1939.
- (68) Smith, R. A. J.; Hartley, R. C.; Murphy, M. P. *Antioxid. Redox Signaling* **2011**, *15*, 3021.
- (69) Rainbolt, T. K.; Atanassova, N.; Genereux, J. C.; Wiseman, R. L. *Cell Metab.* **2013**, *18*, 908.
- (70) Link, C. D. *Proc. Natl. Acad. Sci. U. S. A.* **1995**, *92*, 9368.
- (71) Petrascheck, M.; Ye, X.; Buck, L. B. *Nature* **2007**, *450*, 553.
- (72) Fang-Yen, C.; Gabel, Ch.V.; Samuel, A. D. T.; Bargmann, C. I.; Avery, L. *Methods Cell Biol.* **2012**, *107*, 177.
- (73) Fares, H.; Greenwald, I. *Genetics* **2001**, *159*, 133.
- (74) Maniar, T. A.; Kaplan, M.; Wang, G. J.; Shen, K.; Wei, L.; Shaw, J. E.; Koushika, S. P.; Bargmann, C. I. *Nat. Neurosci.* **2012**, *15*, 48.
- (75) Sekijima, Y.; Wiseman, R. L.; Matteson, J.; Hammarström, P.; Miller, S. R.; Sawkar, A. R.; Balch, W. E.; Kelly, J. W. *Cell* **2005**, *21*, 73.
- (76) Lakowicz, J. R.; Gryczynski, I.; Malak, H.; Gryczynski, Z. *J. Phys. Chem.* **1996**, *100*, 19406.
- (77) Bolton, O.; Kim, J. *J. Mater. Chem.* **2007**, *17*, 1981.
- (78) Reddy, M. A.; Mallesham, G.; Thomas, A.; Srinivas, K.; Rao, V. J.; Bhanuprakash, K.; Giribabu, L.; Grover, R.; Kumar, A.; Kamalasan, M. N.; Srivastava, R. *Synth. Met.* **2011**, *161*, 869.
- (79) Hughes, G.; Kreher, D.; Wang, Ch.; Batsanov, A. S.; Bryce, M. R. *Org. Biomol. Chem.* **2004**, *2*, 3363.
- (80) Oliveira, C. S.; Lira, B. F.; Barbosa-Filho, J. M.; Fernandez Lorenzo, J. G.; Filgueiras de Athayde-Filho, P. *Molecules* **2012**, *17*, 10192.
- (81) Kim, Y. K.; Lee, J. K.; Lee, J. S.; Yoon, C. N.; Chang, Y. T. *Mol. BioSyst.* **2011**, *7*, 2375.
- (82) Gales, L.; Saraiva, M. J.; Damas, A. M. *Biochim. Biophys. Acta* **2007**, *1774*, 59.
- (83) Lima, L. M.; Silva, Vde, A.; Palmieri, Lde, C.; Oliveira, M. C.; Foguel, D.; Polikarpov, I. *Bioorg. Med. Chem.* **2010**, *18*, 100.
- (84) Johnson, S. M.; Connelly, S.; Wilson, I. A.; Kelly, J. W. *J. Med. Chem.* **2009**, *52*, 1115.
- (85) Suydam, I. T.; Snow, C. D.; Pande, V. S.; Boxer, S. G. *Science* **2006**, *313*, 200.
- (86) Sirin, G. S.; Zhou, Y.; Lior-Hoffmann, L.; Wang, S.; Zhang, Y. *J. Phys. Chem. B* **2012**, *116*, 12199.
- (87) Bojarov, P.; Denehy, E.; Walker, I.; Loft, K.; De Souza, D. P.; Woo, L. W. L.; Potter, B. V. L.; McConville, M. J.; Williams, S. J. *ChemBioChem* **2008**, *9*, 613.
- (88) Vane, J. R.; Botting, R. M. *Thromb. Res.* **2003**, *110*, 255.
- (89) Colon, W.; Kelly, J. W. *Biochemistry* **1992**, *31*, 8654.
- (90) Lai, Z.; Colón, W.; Kelly, J. W. *Biochemistry* **1996**, *35*, 6470.
- (91) Connelly, S.; Choi, S.; Johnson, S. M.; Kelly, J. W.; Wilson, I. A. *Curr. Opin. Struct. Biol.* **2010**, *20*, 54.
- (92) Lavis, L. D.; Raines, R. T. *ACS Chem. Biol.* **2014**, *9*, 855.
- (93) Kobayashi, H.; Ogawa, M.; Alford, R.; Choyke, P. L.; Urano, Y. *Chem. Rev.* **2010**, *110*, 2620.